POLITECNICO DI TORINO
Repository ISTITUZIONALE

Charging-Load Prediction for Electric Vehicle Stations Using Correlation Analysis and RIME-CNN-LSTM-Attention Model

Original
Charging-Load Prediction for Electric Vehicle Stations Using Correlation Analysis and RIME-CNN-LSTM-Attention Model / Yang, M., Li, W., Sun, P., Su, X., Huang, T., Zheng, T.. - In: IET GENERATION, TRANSMISSION & DISTRIBUTION. - ISSN 1751-8687. - 20:1(2026). [10.1049/gtd2.70219]

Availability:
This version is available at: 11583/3017576 since: 2026-11-05T10:55:44Z

Publisher:
John Wiley and Sons Inc

Published
DOI:10.1049/gtd2.70219

Terms of use:

This article is made available under terms and conditions as specified in the corresponding bibliographic description in the repository

Publisher copyright

(Article begins on next page)

15 November 2026

Check for updates

IET Generation, Transmission & Distribution

WILEY

The Institution of Engineering and Technology

ORIGINAL RESEARCH OPEN ACCESS

Charging-Load Prediction for Electric Vehicle Stations Using Correlation Analysis and RIME-CNN-LSTM-Attention Model

Mao Yang[1] | Wencheng Li[1] | Peng Sun[1] | Xin Su[1] | Tao Huang[2] | Tianyu Zheng[3]

[1]Key Laboratory of Modern Power System Simulation and Control & Renewable Energy Technology, Ministry of Education (Northeast Electric Power-University), Jilin, China | [2]Department of Energy, Politecnico Di Torino, Torino, Italy | [3]State Grid Jilin Electric Power Co., Ltd, Changchun, China

Correspondence: Peng Sun (sunpeng@neepu.edu.cn)

Received: 26 June 2025 | **Revised:** 24 October 2025 | **Accepted:** 11 December 2025

ABSTRACT

The rapid growth of electric vehicles (EVs) has made accurate forecasting of charging station loads essential for ensuring grid stability and supporting infrastructure planning. While previous studies have investigated this problem, correlation-based feature selection remains relatively underexplored, which may lead to redundant features and reduced prediction accuracy. To address this issue, this paper proposes a hybrid forecasting model, RIME-CNN-LSTM-Attention, which integrates correlation-driven feature selection with advanced deep learning. Pearson, Spearman, and Kendall's tau-b analyses are first applied to identify the most influential factors affecting charging demand. The RIME algorithm is then used to optimise the hyperparameters of the CNN-LSTM network, while the attention mechanism dynamically emphasises critical load fluctuation periods. Case studies utilising actual charging station data illustrate that the proposed model substantially surpasses benchmark methodologies, thereby improving the accuracy and resilience of electric vehicle charging load forecasting.

1 | Introduction

With the aim of achieving the 'carbon peak and carbon neutrality' goals, electric vehicles (EVs) that utilise renewable energy have emerged as crucial tools for advancing the transition towards clean energy. They are expected to be widely adopted and to become commonplace in daily life [1]. However, the rapid growth of EV charging demand is also imposing significant strain on the power system [2]. Therefore, accurate forecasting of EV charging station load is crucial for optimising grid resource scheduling [3, 4], implementing demand-side management [5], and planning charging infrastructure deployment.

To improve the precision of EV charging station load forecasts, it is essential to account for all factors influencing power consumption while continually refining forecasting techniques. Multiple interrelated factors influence the load of EV charging stations. For example, incorporating time-of-use pricing and station utilisation rates has been shown to affect prediction accuracy [6], and integrating weather variables (such as temperature and precipitation) along with traffic data can significantly improve forecasting performance [7, 8]. Other works have identified that driver travel behaviours, initial battery state-of-charge, seasonal variations, and day type (weekday, weekend, or holiday) all impact charging demand [9–11]. These studies demonstrate that considering a broad range of factors can enhance load predictions. However, most of the existing studies did not conduct a comprehensive linear and non-linear correlation analysis on historical data to quantitatively identify the most influential features. Without such analysis and feature selection, models may include variables of weak relevance, which increases complexity and the risk of overfitting.

This is an open access article under the terms of the Creative Commons Attribution License, which permits use, distribution and reproduction in any medium, provided the original work is properly cited.

© 2025 The Author(s). *IET Generation, Transmission & Distribution* published by John Wiley & Sons Ltd on behalf of The Institution of Engineering and Technology.

Prediction methods for EV charging load can be broadly divided into simulation-based, statistical, and machine learning approaches [12]. Simulation methods, such as Monte Carlo and queuing theory, model travel chains, charging behaviours, and station clustering [13–16]. These approaches are useful for scenario analysis but often show weak correlation with actual load data. Statistical learning methods rely on historical charging/discharging records to forecast demand [17]. Examples include integrating road infrastructure and user psychology [18], probabilistic commuting models [19], and traffic data to estimate state of charge and charging demand [20]. While simple to implement, they are constrained by data quality and sample size. Machine learning has become the dominant stream for EV load forecasting due to its ability to capture nonlinear features and temporal dependencies. Early studies applied clustering and SVR [21] or Spark-based multilayer perceptron networks [22]. Later, hybrid models optimised by metaheuristic algorithms, such as NGO-LSTM-SVR, improved parameter tuning and forecasting accuracy [2]. More advanced frameworks combine LSTM with graph neural networks to capture spatial correlations [23] or integrate CNNs to extract local features in time series [24]. Attention mechanisms further enhance interpretability and focus on critical load patterns, as shown in CNN-BiLSTM-Attention models [25, 26]. Despite these advances, existing approaches still struggle with multi-scale temporal modelling, full utilisation of spatial information, and robust interpretability, motivating the development of more comprehensive hybrid frameworks. In addition, recent studies have developed model-free, multi-dimensional, artificial intelligence-based forecasting methods under uncertainty, such as decade-ahead tourism demand [27] and pandemic casualty prediction [28]. These studies demonstrate the potential of artificial intelligence for robust forecasting in complex and uncertain environments. However, such approaches have been primarily applied in non-energy domains, and their application to EV charging station load forecasting remains limited.

In response to the above challenges, this paper proposes a novel hybrid model for electric vehicle charging station load prediction that integrates correlation analysis, the Frost Ice Optimisation Algorithm (RIME), a CNN-LSTM neural network, and an attention mechanism. First, we apply Pearson, Spearman, and Kendall's tau-b correlation analyses to historical data to identify a subset of features that are most strongly correlated with the charging station load. Next, using only these relevant features, we construct a RIME-CNN-LSTM-Attention model: the RIME algorithm is employed to fine-tune the hyperparameters of the CNN-LSTM network, and an attention mechanism is incorporated to highlight key periods of load fluctuation. The main contributions of this work are threefold. First, we establish a comprehensive correlation-analysis-based feature selection framework to determine the most influential factors for EV charging load prediction. Second, we develop a new hybrid forecasting model (RIME-CNN-LSTM-Attention) that combines metaheuristic optimisation (RIME) with deep learning (CNN-LSTM) and an attention mechanism to enhance prediction accuracy. Third, we demonstrate through experiments on real-world charging station data that the proposed model outperforms several baseline methods in predictive accuracy and robustness.

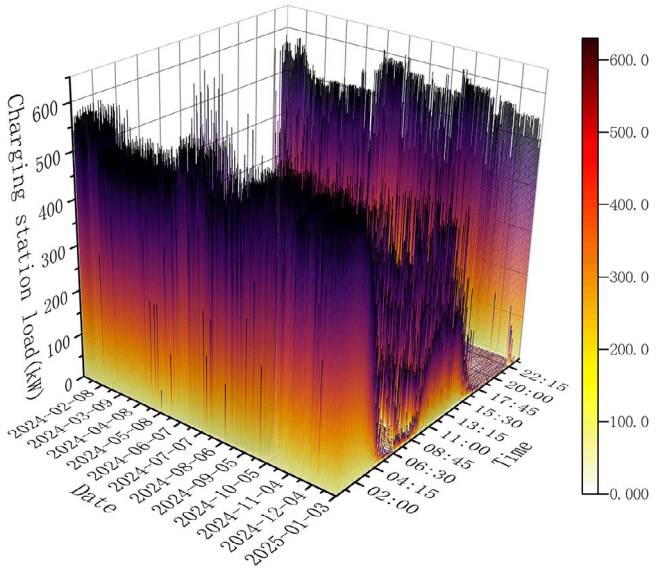


FIGURE 1 | Charging station load power data chart.

2 | Analysis of Load Influencing Factors

2.1 | Data Source

Based on the summary and analysis of previous studies on load-influencing factors, this paper takes temperature, precipitation (snow), air quality, visibility, EV penetration rate, whether it is a weekend, whether it is a holiday, and time-of-use electricity price as influencing factors and conducts correlation analysis with the charging station load [29–31]. All data in this paper are sampled every 15 min from 10 January, 2024, to 3 January, 2025, in a certain city in Jilin Province, with 96 data per day. Temperature, precipitation (snow), air quality, and visibility are derived from the 'Historical Weather Data' platform. The EV penetration rate is determined by dividing the number of electric vehicles by the total number of vehicles in a given city. The time-based electricity rates are provided by the local charging station operator. The load at the charging station is derived from the primary data of the power metering unit, as depicted in Figure 1.

Temperature, rainfall (snow), air quality, and visibility are derived from the 'Historical Weather Data' platform. The level of EV adoption is determined by dividing the total count of EVs within a specific city by the overall number of vehicles. The pricing based on time-of-day rates is set by the local charging station operator. Meanwhile, the power load on the station is obtained from the primary side readings of the energy metering equipment, as shown in Figure 1.

2.2 | Correlation Coefficent

The Pearson correlation coefficient serves as a widely employed statistical metric in data analytics, quantifying the degree of linear association between two continuous variables. This measure not only assesses the intensity of the relationship but also determines whether the variables exhibit a direct or inverse correlation. The value range is [−1, 1]. The closer to −1, the stronger the negative

17518695, 2026, 1, Downloaded from https://ietresearch.onlinelibrary.wiley.com/doi/10.1049/gtd2.70219 by Politecnico Di Torino Sist. Bibl Del Polit Di Torino, Wiley Online Library on [03/11/2026]. See the Terms and Conditions (https://onlinelibrary.wiley.com/terms-and-conditions) on Wiley Online Library for rules of use; OA articles are governed by the applicable Creative Commons License

correlation between the two sets of data, and the closer to 1, indicating negative or positive relationships between the datasets [32].

$$r = \frac{\sum_{i=1}^{n} (x_i - \bar{x})(y_i - \bar{y})}{\sqrt{\sum_{i=1}^{n} (x_i - \bar{x})^2} \sqrt{\sum_{i=1}^{n} (y_i - \bar{y})^2}} \quad (1)$$

The Pearson correlation coefficient, denoted as r, measures the linear relationship between two datasets, $|r| \leq 1$; x_i and y_i are the values of the i-th data point of the two sets of data, respectively; $\bar{x}$ and $\bar{y}$ are the average values of the two sets of data.

Spearman's rank correlation coefficient is a nonparametric measure that assesses the strength and direction of a monotonic association between two variables, whether linear or nonlinear. This statistical tool helps determine if the relationship between datasets is positively or negatively correlated. The value range is also [−1, 1]. The method for computing its numerical value mirrors that of the Pearson correlation coefficient, but after sorting the variable data before calculation, the ranking is used instead of the actual value to calculate the correlation, which reduces the sensitivity to outliers and non-normal distribution data.

$$\rho = 1 - \frac{6 \sum_{i=1}^{n} \left(r_{x_i} - r_{y_i}\right)^2}{n(n^2 - 1)} \quad (2)$$

where ρ is the Spearman correlation coefficient between two sets of data, $|\rho| \leq 1$; r_{x_i} and r_{y_i} are the rankings of the two sets of data $X = (x_1, x_2, \ldots, x_n)$ and $Y = (y_1, y_2, \ldots, y_n)$, respectively.

Kendall's tau-b correlation coefficient is a statistical indicator used to measure the rank correlation between two variables (suitable for measuring nonlinear but monotonic correlation). It assesses the correlation strength between variables by analysing the rank order and consistency across all data pairs. The value range is also [−1, 1].

$$\tau = \frac{n_c - n_d}{\sqrt{(n_c + n_d + t_x)(n_c + n_d + t_y)}} \quad (3)$$

where τ is the Kendall's tau-b correlation coefficient between two sets of data, $|\tau| \leq 1$; n_c is the number of pairs of points with consistent order ($x_i > x_j$ and $y_i > y_j$, or $x_i < x_j$ and $y_i < y_j$); n_d is the number of pairs of points with inconsistent order ($x_i > x_j$ and $y_i < y_j$, or $x_i < x_j$ and $y_i > y_j$); t_x is the number of pairs of points in variable X where equality occurs; t_y is the number of pairs of points in variable Y where equality occurs.

2.3 | Correlation Analysis

Based on the three correlation coefficient calculation principles in Section 2.2, the SPSS 25.0 statistical software was used to obtain the Pearson, Spearman, and Kendall's tau-b correlation coefficients of temperature, precipitation (snow), air quality, visibility, EV penetration rate, whether it is a weekend, whether it is a holiday, time-of-use electricity price, and EV charging station load. Statistical significance was evaluated at the 1% ($p < 0.01$) and 5% ($p < 0.05$) levels. The correlation coefficients themselves serve as effect sizes, reflecting both the strength and direction of associations between influencing factors and charging load. The results are summarised in Table 1, and the correlation heat map between the variables is shown in Figure 2.

TABLE 1 | Correlation coefficients between various factors and EV charging station load.

Influencing factors	Methods		
	Pearson	Spearman	Kendall's tau-b
Temperature	−0.110**	−0.195**	−0.131**
Precipitation (snow)	−0.022**	−0.044**	−0.036**
Air quality	−0.051**	0.013*	0.012*
Visibility	−0.063**	−0.030**	−0.020*
EV penetration rate	0.026**	0.138**	0.011**
Weekend	−0.003	−0.005	−0.007
Holiday	−0.005	−0.017*	−0.014*
Time-of-day electricity price	−0.536**	−0.491**	−0.377**

Note: The '**' or '*' symbols marked in the upper right corner of the correlation coefficient represent statistical significance at the 1% and 5% levels, respectively. If there is no '**' or '*', it fails the significance test, indicating that there is no correlation between the variables.

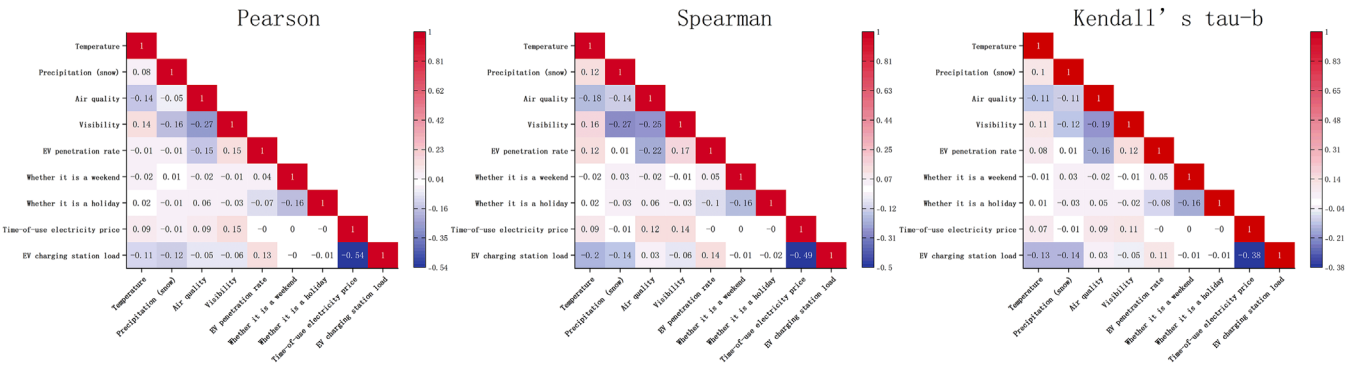
As indicated in Table 1 and Figure 2, the load at EV charging stations is most heavily affected by the time-of-use electricity pricing (all three correlation coefficients show a high negative correlation and are at the 0.01 significance level), followed by temperature, precipitation (snow), air quality, visibility, and EV penetration rate (the three correlation coefficients are not high but are all at the 0.01 or 0.05 significance level). Whether it is a weekend or a holiday has a weaker impact on the load (all three correlation coefficients are low, and some are significant at the 0.05 significance level). Therefore, six factors, including temperature, precipitation (snow), air quality, visibility, EV penetration rate, and time-of-use electricity price, are selected as the characteristic data of the prediction model.

3 | Principles of Algorithms and Models

3.1 | RIME Optimisation Algorithm

The RIME optimisation algorithm (RIME) is a parameter optimisation algorithm based on the physical phenomenon of frost ice proposed by Su Hang in 2023 [33]. Its core inspiration comes from the growth and aggregation behaviour of frost ice in nature. The algorithm is based on swarm intelligence. By simulating the random diffusion and regular puncture mechanism of 'frost ice' in a low-temperature environment, it effectively combines global search and local development capabilities to achieve efficient optimisation of model parameters. Compared with classic algorithms such as PSO, WOA, HHO, and MFO, RIME has a fast convergence speed, can more effectively balance resource exploration and utilisation, and has stronger optimisation capabilities

17518695, 2026, 1, Downloaded from https://ietresearch.onlinelibrary.wiley.com/doi/10.1049/gtd2.70219 by Politecnico Di Torino Sist. Bibl Del Polit Di Torino, Wiley Online Library on [03/11/2026]. See the Terms and Conditions (https://onlinelibrary.wiley.com/terms-and-conditions) on Wiley Online Library for rules of use; OA articles are governed by the applicable Creative Commons License



(a) Pearson (b) Spearman (c) Kendall's tau-b

FIGURE 2 | Correlation thermogram.

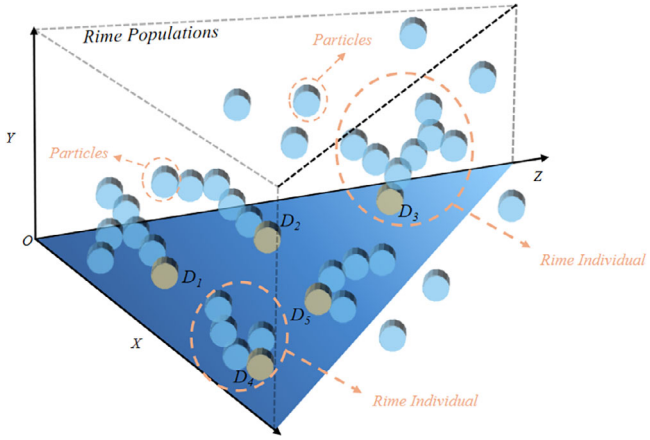


FIGURE 3 | Initialisation of the rime space.

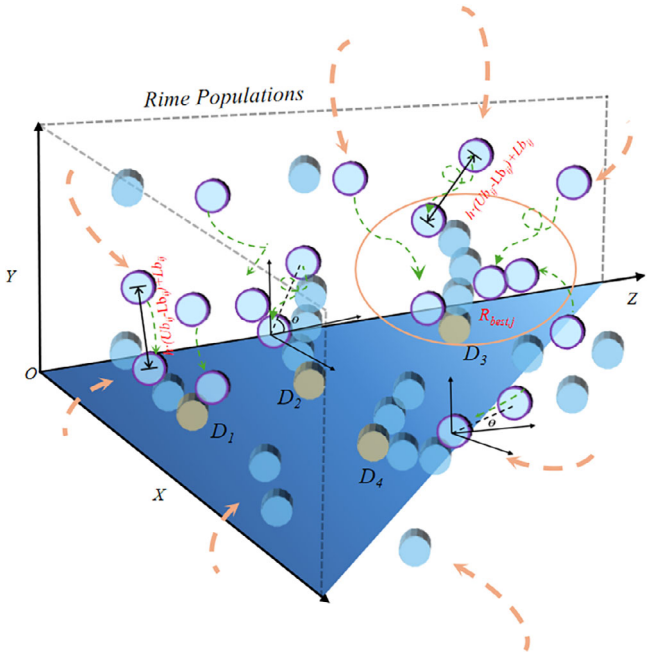


FIGURE 4 | Soft-rime particles motion.

and higher stability when facing complex problems [34]. Thus, the study employs the RIME method for fine-tuning CNN and LSTM network parameters, enhancing the model's data fitting and boosting prediction precision.

RIME consists of four stages: frost cluster initialisation, soft frost search, hard frost puncture, and active greedy selection.

Frost cluster initialisation: Each 'frost particle' represents a candidate solution (i.e., a parameter vector), and all frost particles constitute a search population. In the initialisation stage, the frost cluster R is established by randomly generating initial solutions in the parameter space, as shown in Formula (4), and the corresponding structure is shown in Figure 3.

$$R = \begin{bmatrix} x_{11} & x_{12} & \cdots & x_{1d} \\ x_{21} & x_{22} & \cdots & x_{2d} \\ \vdots & \vdots & \ddots & \vdots \\ x_{n1} & x_{n2} & \cdots & x_{nd} \end{bmatrix} \tag{4}$$

where x_{nd} represents the d-th parameter value of the n-th individual, d is the parameter dimension, and n is the population size.

Soft frost search strategy: In nature, soft frost ice exhibits slow, random, and diffuse free growth characteristics. RIME uses this characteristic to design a global search strategy that enables individuals to perform angled jump diffusion around the current optimal solution to improve the coverage of the search. The calculation formulas are shown in Formulas (5)–(8), and the corresponding structure is shown in Figure 4.

$$R_{ij}^{new} = R_{best,j} + r_1 \cdot \cos\theta \cdot \beta \cdot \left(h \cdot \left(Ub_{ij} - Lb_{ij}\right) + Lb_{ij}\right), r_2 < E \tag{5}$$

$$\theta = \pi \cdot \frac{t}{10 \cdot T} \tag{6}$$

$$\beta = 1 - \left(\frac{\omega \cdot t}{T}\right)/\omega \tag{7}$$

$$E = \sqrt{\frac{t}{T}} \tag{8}$$

17518695, 2026, 1, Downloaded from https://ietresearch.onlinelibrary.wiley.com/doi/10.1049/gtd2.70219 by Politecnico Di Torino Sist. Bibl Del Polit Di Torino, Wiley Online Library on [03/11/2026]. See the Terms and Conditions (https://onlinelibrary.wiley.com/terms-and-conditions) on Wiley Online Library for rules of use; OA articles are governed by the applicable Creative Commons License

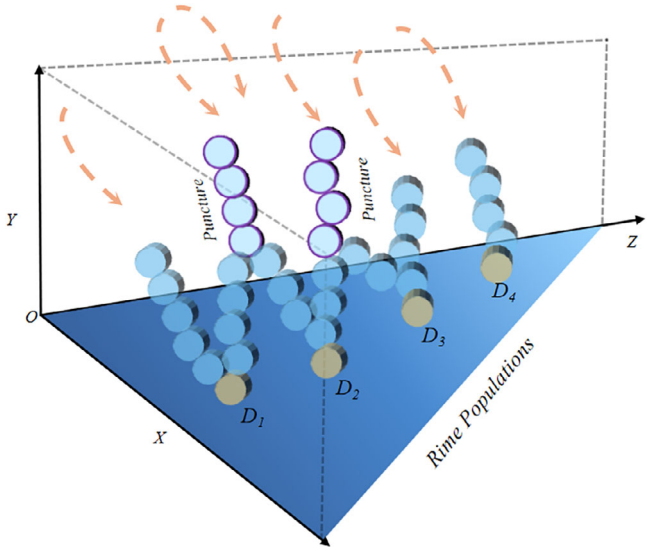


FIGURE 5 | Hard-rime puncturing.

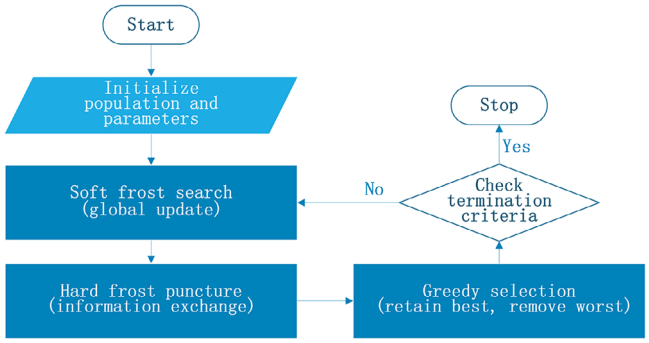


FIGURE 6 | Structure diagram of RIME.

where $R_{\text{best,j}}$ is the new position of the particle after updating; r_1 is a random number in the range of (−1, 1); t is the current iteration number; T is the maximum number of iterations of the algorithm; β is the environmental factor; ω is the number of segments used to control the step function; h is a random number in the range of (0, 1); Ub_{ij} and Lb_{ij} are the upper and lower limits of each parameter; r_2 is a random number in the range of (0, 1); and E is the adhesion coefficient.

Hard frost puncture mechanism: Unlike soft frost, hard frost is affected by strong winds and has the characteristics of strong directionality and rapid accumulation. RIME simulates the continuous and rapid growth of hard frost in a specific direction through the "puncture mechanism" to enhance local development capabilities. The calculation formula is shown in Formula (9), and the puncture phenomenon is shown in Figure 5.

$$R_{\text{ij}}^{\text{new}} = R_{\text{best,j}}, r_3 < F^{\text{normr}}\left(S_{\text{j}}\right) \tag{9}$$

where r_3 is a random number in the range of (0, 1); $F^{\text{normr}}(S_{\text{j}})$ is the normalised value of the current agent fitness value.

Active greedy selection mechanism: Check whether the agent's revised fitness score outperforms the existing global benchmark. Should it prove superior, update the global optimum with this new value and designate the corresponding agent as the top performer.

The RIME structure diagram is shown in Figure 6.

The rationale for selecting RIME in this study lies in its superior capability to address the hyperparameter optimisation challenge inherent in the complex CNN-LSTM-Attention model. The hyperparameter search space, encompassing parameters such as learning rate, kernel size, and the number of hidden neurones, is typically high-dimensional and non-convex. Traditional gradient-based optimisers are prone to becoming trapped in local optima, while other metaheuristic algorithms may struggle with balancing exploration and exploitation or suffer from premature convergence. RIME's soft frost search strategy, characterised by its angled jump diffusion, facilitates extensive exploration in the early stages, effectively scanning a broader solution space. Subsequently, the hard frost puncture mechanism, guided by fitness values, allows for precise exploitation in promising regions. This dynamic and adaptive search behaviour makes RIME particularly well-suited for identifying a near-optimal hyperparameter configuration for our deep learning model, thereby enhancing both predictive accuracy and training stability.

3.2 | Convolutional Neural Network

Convolutional neural network (CNN) is a foundational deep learning method [35]. Thanks to incorporating local correlations and shared weights, CNNs efficiently handle raw data at a superior and more conceptual level [36]. The core of its neural architecture is a tapestry woven with convolutional, pooling, and fully connected layers. This arrangement slashes the number of weights, simplifies the network's complexity, and elevates the fidelity of the data features [37]. Therefore, the study employs a CNN for local feature extraction from the input data, subsequently downsizes the dimensions, and feeds the resultant features into an LSTM network.

Convolution layer: extracts local features of input data by sliding a convolution kernel. The calculation formula is shown in Formula (10).

$$Y(i,j) = \sum_{\text{m=0}}^{f-1}\sum_{\text{n=0}}^{f-1} \text{X}(i+m, j+n)\cdot \text{K}(m,n) + b \tag{10}$$

where $Y(i, j)$ is the value of the output at position (i, j); K is the convolution kernel of size $f \times f$; X$(i + m, j + n)$ is the value of the input at position (i, j); K(m, n) is the weight of the convolution kernel; and b is the bias term.

Pooling layer: Perform the maximum pooling operation on the input data. The calculation formula is shown in Formula (11).

$$Y(i,j) = \max X(m,n), m \in [i, i+\text{p}-1], \text{n} \in [j, j+\text{p}-1] \tag{11}$$

where $Y(i, j)$ is the value of the output at position (i, j) after pooling and $X(m, \text{n})$ is the input data.

17518695, 2026, 1, Downloaded from https://ietresearch.onlinelibrary.wiley.com/doi/10.1049/gtd2.70219 by Politecnico Di Torino Sist. Bibl Del Polit Di Torino, Wiley Online Library on [03/11/2026]. See the Terms and Conditions (https://onlinelibrary.wiley.com/terms-and-conditions) on Wiley Online Library for rules of use; OA articles are governed by the applicable Creative Commons License

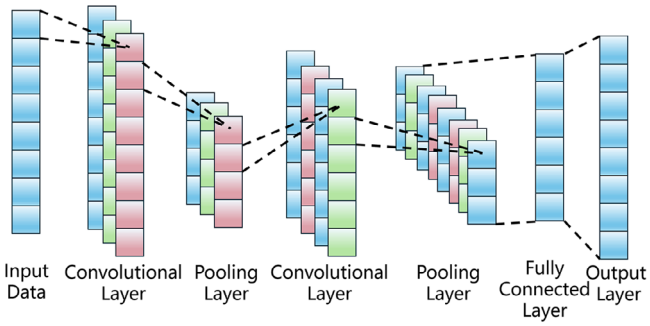


FIGURE 7 | Structure diagram of CNN.

Fully connected layer: maps the input to the target space according to the weights. The calculation formula is shown in Formula (12).

$$y = W \cdot X + b \tag{12}$$

where y is the output of the fully connected layer, W is the weight matrix of the fully connected layer, x is the input data, and b is the bias term.

The CNN structure diagram is shown in Figure 7.

3.3 | Long Short-Term Memory Network

Long short-term memory (LSTM) is a special type of recurrent neural network (RNN) that aims to solve the problem of gradient vanishing or exploding defects encountered by standard RNN when processing long sequences [38]. The LSTM architecture manages the flow of data with the help of three key gating mechanisms—the input, forget, and output gates. This setup is crucial for capturing those long-term dependencies, ensuring that the history of load sequences is maintained over time. In the mix, the forget gate holds onto the relevant information, keeping out the old, irrelevant info from the last tick. Meanwhile, the input and output gates handle the data, sifting through and passing along the refined info to the next phase. The calculation formulas are shown in Formula (13)–(18).

$$f_t = \sigma\left(W_{fx}x_t + W_{fh}h_{t-1} + b_f\right) \tag{13}$$

$$i_t = \sigma\left(W_{ix}x_t + W_{ih}h_{t-1} + b_i\right) \tag{14}$$

$$g_t = \tanh\left(W_{gx}x_t + W_{gh}h_{t-1} + b_g\right) \tag{15}$$

$$o_t = \sigma\left(W_{ox}x_t + W_{oh}h_{t-1} + b_o\right) \tag{16}$$

$$S_t = S_{t-1}\, f_t + i_t\, g_t \tag{17}$$

$$h_t = \tanh(S_t)o_t \tag{18}$$

where σ is the sigmoid activation function; W_{fx}, W_{fh}, W_{ix}, W_{ih}, W_{gx}, W_{gh}, W_{ox}, and W_{oh} are weight matrices; x_t is the input at the current moment; h_{t-1} is the intermediate state of the previous moment; b_f, b_i, b_g, and b_o are the bias terms; f_t is the output of the forget gate; i_t is the output of the input gate; g_t is the candidate memory cell; o_t is the output of the output gate; S_t is the unit state; S_{t-1} is the unit state at the previous moment; h_t is the intermediate state.

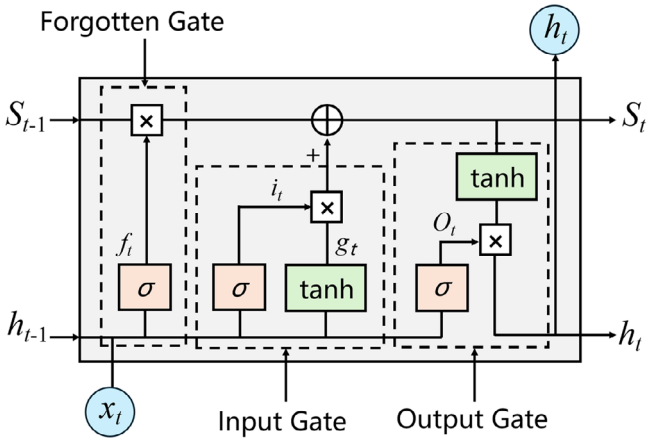


FIGURE 8 | Structure diagram of LSTM.

The LSTM structure diagram is shown in Figure 8.

3.4 | Attention Mechanism

The attention mechanism is a concept rooted in natural language processing research, image detection, speech recognition, and computer technology [39]. It can dynamically adjust the degree of attention according to the characteristics of different input data and increase the attention to the weight of important information, as well as minimise the impact of unrelated data. Therefore, this paper uses the attention mechanism to help the model automatically identify which features are most important in predicting EV charging power and dynamically adjust the degree of attention to different input data. The calculation formula is shown in Formulas (19)–(20).

$$\alpha_n = p(z = n|X, q) = \mathrm{softmax}\left(s\left(x_n, q\right)\right) = \frac{\exp\left(s\left(x_n, q\right)\right)}{\sum_{j=1}^{N} s\left(x_j, q\right)} \tag{19}$$

$$\mathrm{Attention}\left(X, q\right) = \sum_{n=1}^{N} a_n x_n \tag{20}$$

where X is a vector sequence containing N elements, q is the query vector, a_n is the weight of the n-th element, $s(x_n, q)$ is the attention score function, and attention(X, q) is the attention vector.

The illustration of the attention mechanism's framework can be observed in Figure 9.

4 | RIME-CNN-LSTM-Attention Model

4.1 | Building CNN-LSTM-Attention Model

The CNN-LSTM-Attention architecture employs CNN for local feature extraction and LSTM for identifying long-term data dependencies, and the attention mechanism to optimise the weighting of important information, so that the model can

17518695, 2026, 1, Downloaded from https://ietresearch.onlinelibrary.wiley.com/doi/10.1049/gtd2.70219 by Politecnico Di Torino Sist. Bibl Del Polit Di Torino, Wiley Online Library on [03/11/2026]. See the Terms and Conditions (https://onlinelibrary.wiley.com/terms-and-conditions) on Wiley Online Library for rules of use; OA articles are governed by the applicable Creative Commons License

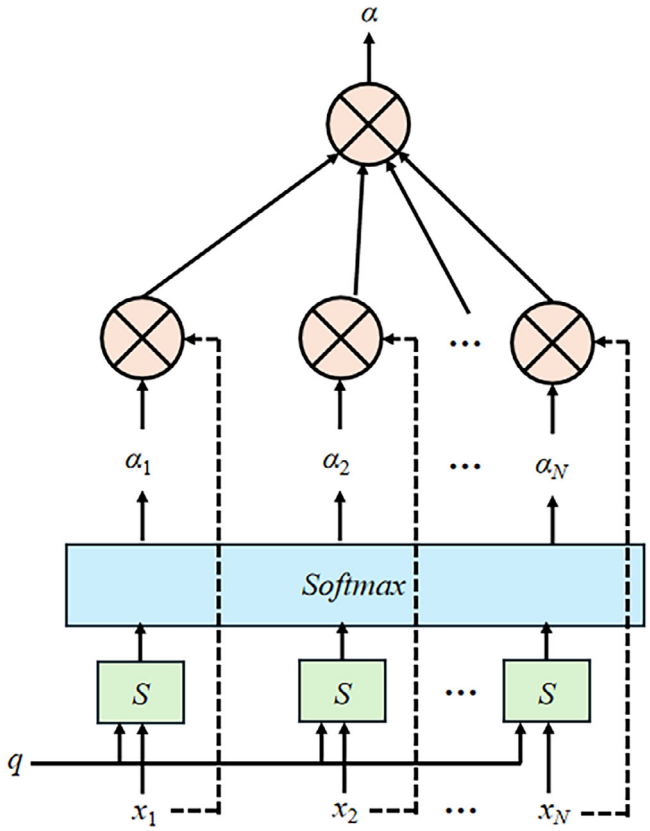


FIGURE 9 | Structure diagram of attention mechanism.

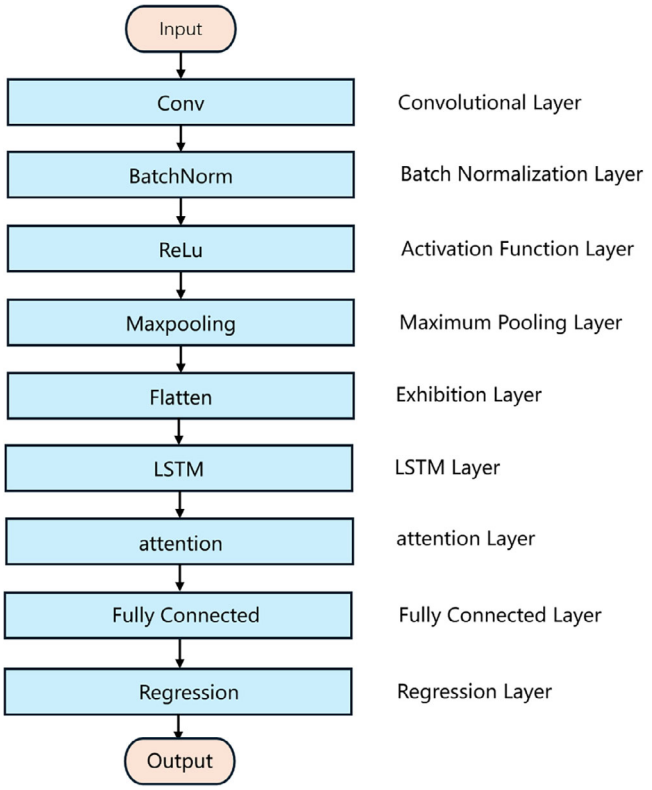


FIGURE 10 | Structure diagram of CNN-LSTM-Attention model.

efficiently process complex time series data and make accurate predictions. Figure 10 illustrates the model's structural framework developed in this study.

Initially, the dataset serves as the entry point for processing. Subsequently, the convolutional layer employs an assortment of filters to adeptly combine various feature signals and derive the initial set of data attributes. The batch normalisation layer standardises the input so that the mean of each channel is 0 and the variance is 1. The activation function layer applies nonlinear activation to the input data, setting all negative values to 0 and keeping the positive values unchanged. The max pooling layer processes input data by extracting the highest values within defined regions. Next, the flattening layer reshapes multidimensional data into a single continuous vector. For sequential data, the LSTM layer captures temporal patterns and dependencies over time. The attention mechanism then dynamically prioritises different segments of the input, enhancing feature representation. Following this, the dense layer projects the processed data into the desired output space using learnt weight distributions. Finally, the regression layer evaluates the model's predictions against ground truth values, computes the loss based on prediction errors, and propagates adjustments backward to fine-tune the network's parameters.

4.2 | RIME Optimises Model Parameters

In traditional CNN-LSTM-Attention, training usually relies on gradient descent optimisation methods (such as Adam or SGD), which can get stuck in local optima or slow convergence. Consequently, this paper introduces the RIME algorithm, which uses its unique frost diffusion mechanism to optimise network parameters, search for optimal solutions more effectively in a multi-dimensional solution space, reduce the impact of local optimal solutions, and improve global search capabilities. In this framework, RIME generates candidate hyperparameter sets (such as learning rate, kernel size, and hidden neurones), evaluates them through the CNN-LSTM-Attention model using prediction errors (MAE, RMSE, MAPE) as the fitness function, and iteratively updates the parameters until convergence. The best-performing hyperparameters are then fed back into the CNN-LSTM-Attention network, ensuring a clear closed-loop flow between the optimisation process and the deep learning layers. Figure 11 illustrates the architecture of the developed RIME-CNN-LSTM-Attention model.

The steps for running this model are as follows:

1. Construct the CNN-LSTM-Attention model framework to capture temporal–spatial features of the load data.
2. Initialise the parameters of the RIME algorithm, including population size, maximum iteration count, soft frost coefficients, and the search ranges for learning rate, convolution kernel size, and hidden neurone number.
3. Generate the initial frost cluster (solution population) to provide diverse candidate parameter sets.
4. Apply the soft frost search, hard frost puncture, and greedy selection strategies to iteratively update particles' positions and fitness, while maintaining the global best solution.

17518695, 2026, 1, Downloaded from https://ietresearch.onlinelibrary.wiley.com/doi/10.1049/gtd2.70219 by Politecnico Di Torino Sist. Bibl Del Polit Di Torino, Wiley Online Library on [03/11/2026]. See the Terms and Conditions (https://onlinelibrary.wiley.com/terms-and-conditions) on Wiley Online Library for rules of use; OA articles are governed by the applicable Creative Commons License

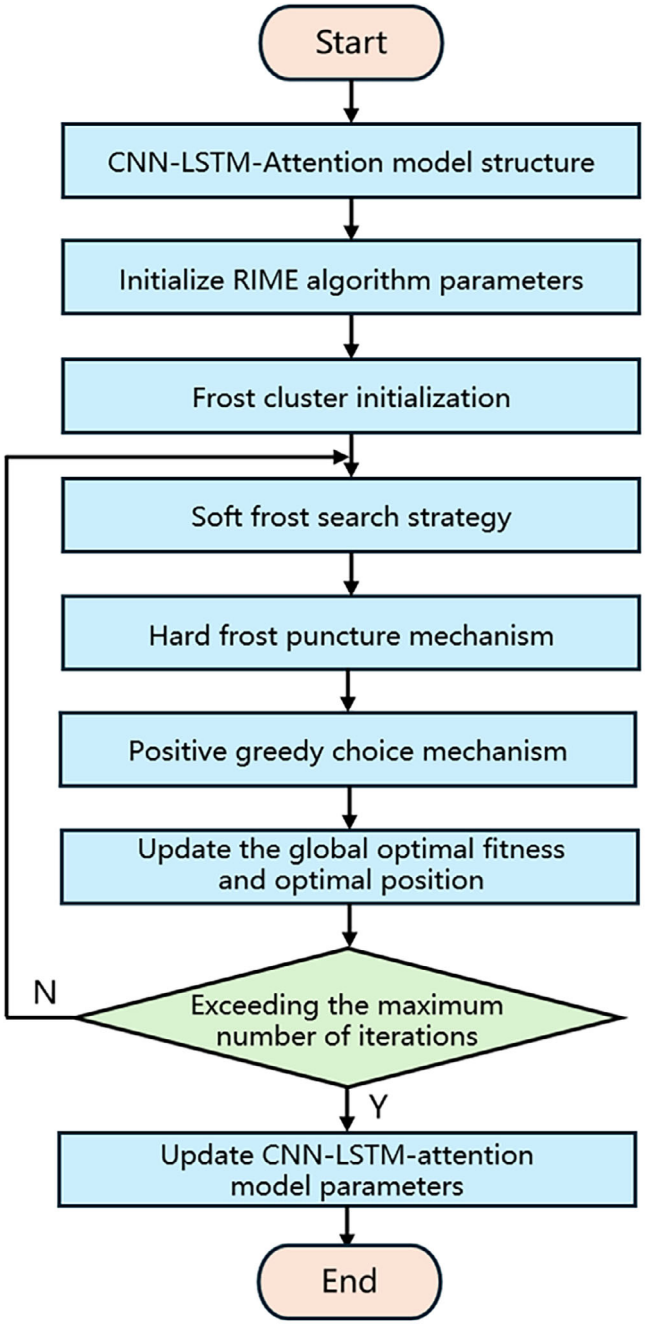


FIGURE 11 | Structure diagram of RIME-CNN-LSTM-Attention model.

5. Check the iteration condition. If the maximum number of iterations is not reached, return to step (4); otherwise, stop the search.
6. Use the globally optimal hyperparameters obtained by RIME to update and train the CNN-LSTM-Attention model, forming the final optimised forecasting structure.

Importantly, the RIME algorithm optimises key hyperparameters—such as the number and size of convolutional kernels, the number of hidden units in the LSTM layer, and the learning rate. Through its distinctive soft frost search strategy and hard frost puncture mechanism, RIME effectively balances global exploration and local exploitation in the hyperparameter space. This optimisation strategy mitigates the risk of the CNN-LSTM-Attention model becoming trapped in local optima—a common limitation of traditional gradient-based methods—and facilitates the discovery of hyperparameter configurations that yield superior overall performance.

4.3 | Uncertainty Analysis and Mitigation Strategies

EV charging load forecasting is inherently affected by multiple sources of uncertainty, which can compromise predictive accuracy and model robustness. This section categorises the primary types of uncertainty and outlines how the proposed model is designed to mitigate them within its architectural and optimisation framework:

1. Input feature uncertainty
   This stems from data noise, missing values, and the inclusion of irrelevant or weakly correlated features, which may introduce overfitting or reduce model generalisation. As discussed in Section 2, a correlation-based feature selection process is applied during pre-processing to retain only statistically significant and meaningful inputs (e.g., time-of-use electricity price, temperature). This filtering reduces input noise and enhances the signal quality, strengthening model focus and interpretability.
2. Temporal dynamic uncertainty
   EV charging load exhibits complex, volatile temporal patterns characterised by sudden peaks and valleys driven by collective, stochastic user behaviour. The key challenge is that the importance of historical information for making the next prediction is not fixed but varies over time. The CNN-LSTM-Attention architecture captures both short-term fluctuations and long-term dependencies. CNN layers extract local patterns; LSTM layers model sequential trends; and the attention mechanism dynamically re-weights historical time steps, allowing the model to adaptively prioritise critical periods for accurate prediction.
3. Model configuration uncertainty
   Deep learning models are sensitive to hyperparameter settings (e.g., learning rate, kernel size, number of hidden units), which significantly influence training stability and predictive power. Poor configuration may cause convergence failures or overfitting. The RIME optimisation algorithm addresses this challenge by framing hyperparameter tuning as a global optimisation task. Through its hybrid strategy—combining soft frost search and hard frost puncture—RIME effectively searches the high-dimensional parameter space, avoiding suboptimal local minima and yielding stable, high-performing model configurations.

5 | Case Analysis

5.1 | Data Set and Model Parameters

To validate the scientific rigour and dependability of the proposed method, this case study leverages load power data alongside

17518695, 2026, 1, Downloaded from https://ietresearch.onlinelibrary.wiley.com/doi/10.1049/gtd2.70219 by Politecnico Di Torino Sist. Bibl Del Polit Di Torino, Wiley Online Library on [03/11/2026]. See the Terms and Conditions (https://onlinelibrary.wiley.com/terms-and-conditions) on Wiley Online Library for rules of use; OA articles are governed by the applicable Creative Commons License

meteorological data, building on the correlation analysis findings outlined in Section 1.3 (temperature, precipitation (snow), air quality, visibility, EV integration percentage and real-time energy tariffs) at a major charging facility, boasting a 2.5 MW capacity, within Jilin Province. The collection time is from 10 January, 2024, to 3 January, 2025, with a sampling interval of 15 min, for a total of 34,560 data. The model parameters are as follows [40–42]: The optimisation setup employs 2 search agents with a cap of 10 iterations. Key parameters include a soft frost value of 5, learning rates bounded between 0.001 and 0.01, convolution kernel sizes ranging from 2 to 5, and hidden layer neurones constrained to 50–60 units. The model undergoes 400 training epochs for thorough convergence.

5.2 | Evaluation Indicators

To assess how well the proposed algorithm and the benchmark algorithms perform in terms of predictive accuracy [43, 44], this example uses mean absolute error (MAE) [45], root mean square error (RMSE), and mean absolute percentage error (MAPE) [46] as evaluation indicators. The calculation formulas of each evaluation indicator are shown in Formula (21)–(23).

$$L_{MAE} = \frac{1}{n}\sum_{i=1}^{n}|\hat{y}_i - y_i| \tag{21}$$

$$L_{RMSE} = \sqrt{\frac{1}{n}\sum_{i=1}^{n}(\hat{y}_i - y_i)^2} \tag{22}$$

$$L_{MAPE} = \frac{1}{n}\sum_{i=1}^{n}\frac{|\hat{y}_i - y_i|}{y_i} \times 100\% \tag{23}$$

where n is the number of detection points; $\hat{y}_i$ and y_i are the predicted load data and actual data in the test set.

5.3 | Case Study Results Analysis

This paper adopts the RIME-CNN-LSTM-Attention model, takes 288 sampling points as a data set, takes 118 feature data sets of 354 days from 10 January to 28 December, 2024, as the input of the training set, takes 118 load data sets of 354 days from 13 January to 31 December, 2024, as the output training model of the training set, and takes 1 feature data set of 3 days from 29 December to 31 December, 2024, as the input of the test set, and predicts the load data from 1 January to 3 January, 2025. The prediction results are shown in Figure 12. The MAPE iterative change curve after the RIME process is shown in Figure 13. It can be seen from Figures 12 and 13 that the predicted data is basically consistent with the actual load, and the MAPE is further reduced by continuously optimising the model parameters through RIME.

5.4 | Comparative Analysis of Different Prediction Models

To assess the performance of the newly developed RIME-CNN-LSTM-Attention model, we conducted a comparative analysis with several alternative architectures—including CNN-LSTM-Attention, CNN-Attention, LSTM-Attention, CNN—for predicting charging station demand over a three-day period, 1 January to 3 January, 2025. Figure 14 displays the comparison outcomes, while Table 2 presents the quantitative results for each model.

As shown in Table 2, compared with the CNN-LSTM-Attention, CNN-Attention, LSTM-Attention, and CNN models, the MAE of the proposed RIME-CNN-LSTM-Attention model decreased by 68.47, 334.32, 431.42, and 801.28; the RMSE decreased by 6.22, 29.54, 39.43, and 67.91; and the MAPE decreased by 1.45%, 7.07%, 9.13%, and 16.95%, respectively. Although the RIME-CNN-LSTM-Attention requires slightly longer training due to the optimisation procedure, the runtime remains within a practical range, demonstrating its feasibility and applicability in real-world forecasting tasks.

5.5 | Verification of Feature Screening Effect

To verify the role of feature screening in load forecasting, this paper builds a model based on the six factors strongly related to load (temperature, precipitation (snow), air quality, visibility, EV penetration, and time-of-use electricity price) screened in Section 1.3 and compares the modelling results with those without feature screening and using all eight original feature factors. Both models use the RIME-CNN-LSTM-Attention architecture, and other parameter settings remain consistent to ensure fairness in the comparison. The comparison results are shown in Figure 15. Table 3 presents the findings of the quantitative analysis.

As can be seen from Table 3, after feature screening, the prediction indicators of the model are significantly optimised, among which MAE is reduced from 218.42 kW to 152.11 kW, RMSE is reduced from 19.65 kW to 12.58 kW, and MAPE is reduced from 4.62% to 3.22%. This shows that eliminating redundant features with little impact on load through correlation analysis can help reduce interference factors in model training and improve the effectiveness of feature extraction, thereby enhancing the model's prediction precision and its capacity to generalise tests.

5.6 | Long-Term Forecasting Capability Analysis and Comparison

To further assess the RIME-CNN-LSTM-Attention model's generalisation and stability for long-term load forecasting, this paper selects different forecast days (3 days, 6 days, and 15 days) for comparative experiments, keeping the model structure and parameter settings consistent and only adjusting the input data and forecast period range. The model prediction results of each forecast period are shown in Figure 16, and Table 4 summarises the quantitative assessment metrics.

Table 4 shows that with more forecast days, the model's error metrics (MAE, RMSE, and MAPE) all tend to rise accordingly, indicating that the expansion of the time span places higher requirements on the model and the forecast difficulty increases accordingly. However, even in a 15-day forecast period, the RIME-CNN-LSTM-Attention model can still maintain a low error level (MAE is 953.72 kW, RMSE is 87.34 kW, and MAPE is 7.38%), indicating that it has strong long-term forecasting capabilities and robust model performance.

17518695, 2026, 1, Downloaded from https://ietresearch.onlinelibrary.wiley.com/doi/10.1049/gtd2.70219 by Politecnico Di Torino Sist. Bibl Del Polit Di Torino, Wiley Online Library on [03/11/2026]. See the Terms and Conditions (https://onlinelibrary.wiley.com/terms-and-conditions) on Wiley Online Library for rules of use; OA articles are governed by the applicable Creative Commons License

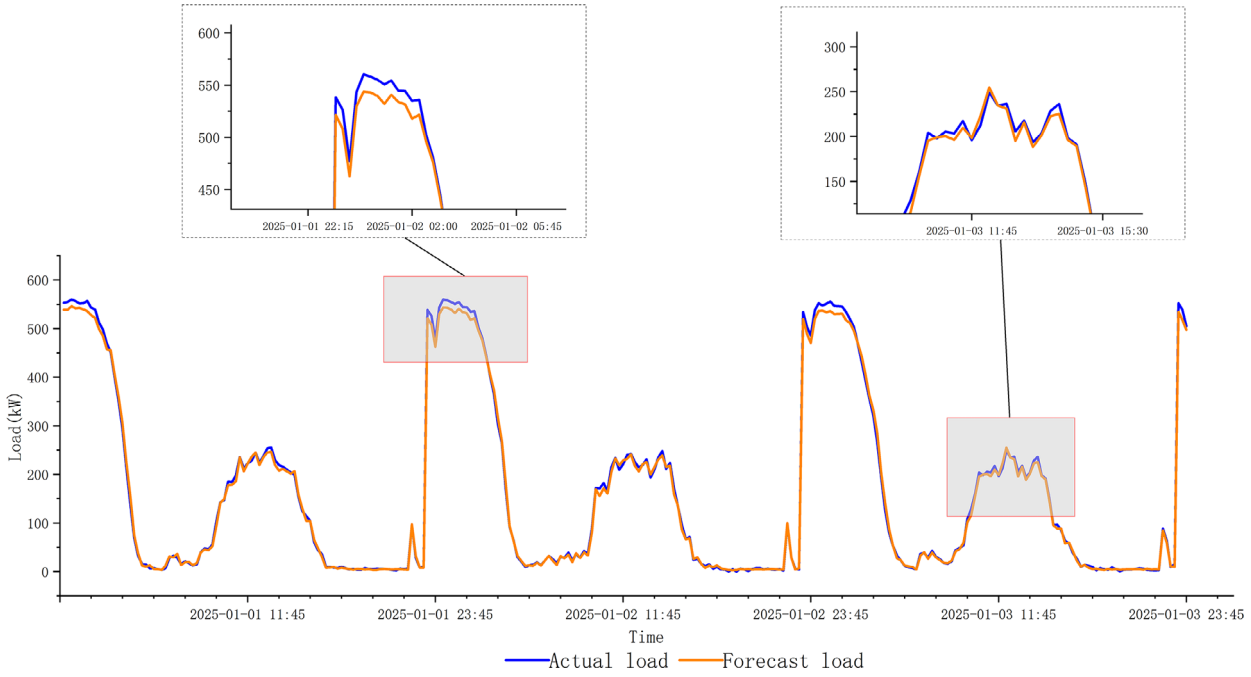


FIGURE 12 | Prediction results of the model proposed.

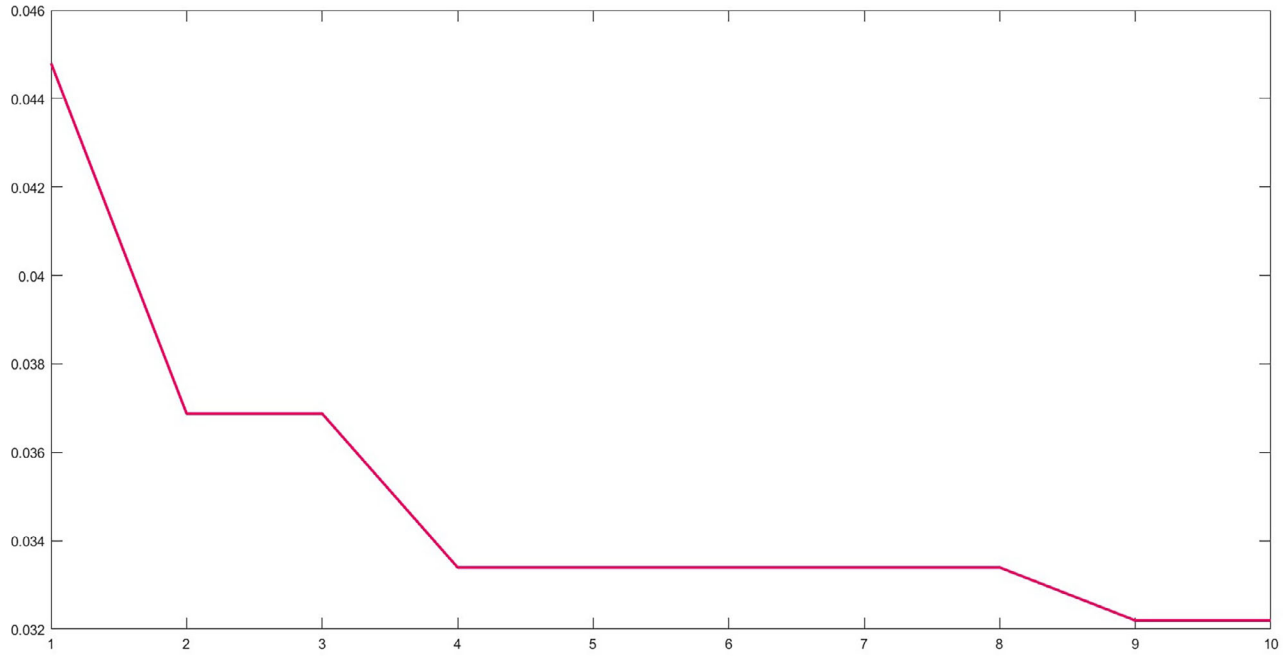


FIGURE 13 | MAPE iteration change curve.

TABLE 2 | Comparison of prediction errors of each model.

Model	MAE (kW)	RMSE (kW)	MAPE (%)	Runtime (s)
RIME-CNN-LSTM-Attention	152.11	12.58	3.22	138.4
CNN-LSTM-Attention	220.58	18.80	4.67	111.6
CNN-Attention	486.43	42.12	10.29	95.2
LSTM-Attention	583.53	52.01	12.35	102.7
CNN	953.39	80.49	20.17	84.5

Note: The runtime refers to the average training and validation time per experiment on the same computational platform (Intel i5 CPU, 16 GB RAM).

17518695, 2026, 1, Downloaded from https://ietresearch.onlinelibrary.wiley.com/doi/10.1049/gtd2.70219 by Politecnico Di Torino Sist. Bibl Del Polit Di Torino, Wiley Online Library on [03/11/2026]. See the Terms and Conditions (https://onlinelibrary.wiley.com/terms-and-conditions) on Wiley Online Library for rules of use; OA articles are governed by the applicable Creative Commons License

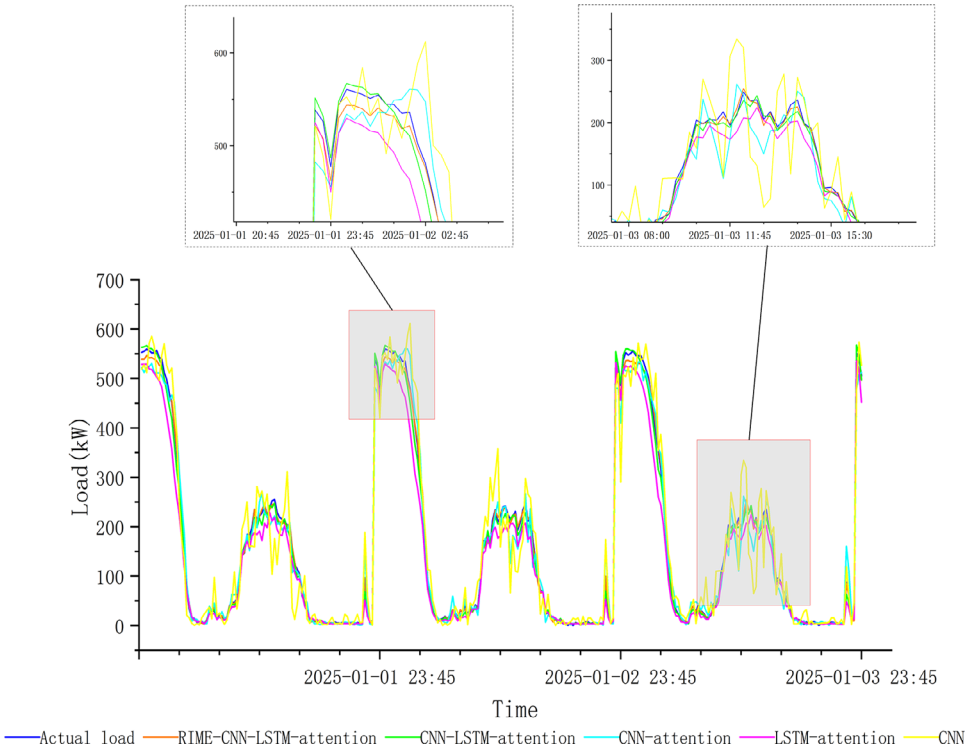


FIGURE 14 | Comparison of the predicted values of the proposed model with other models.

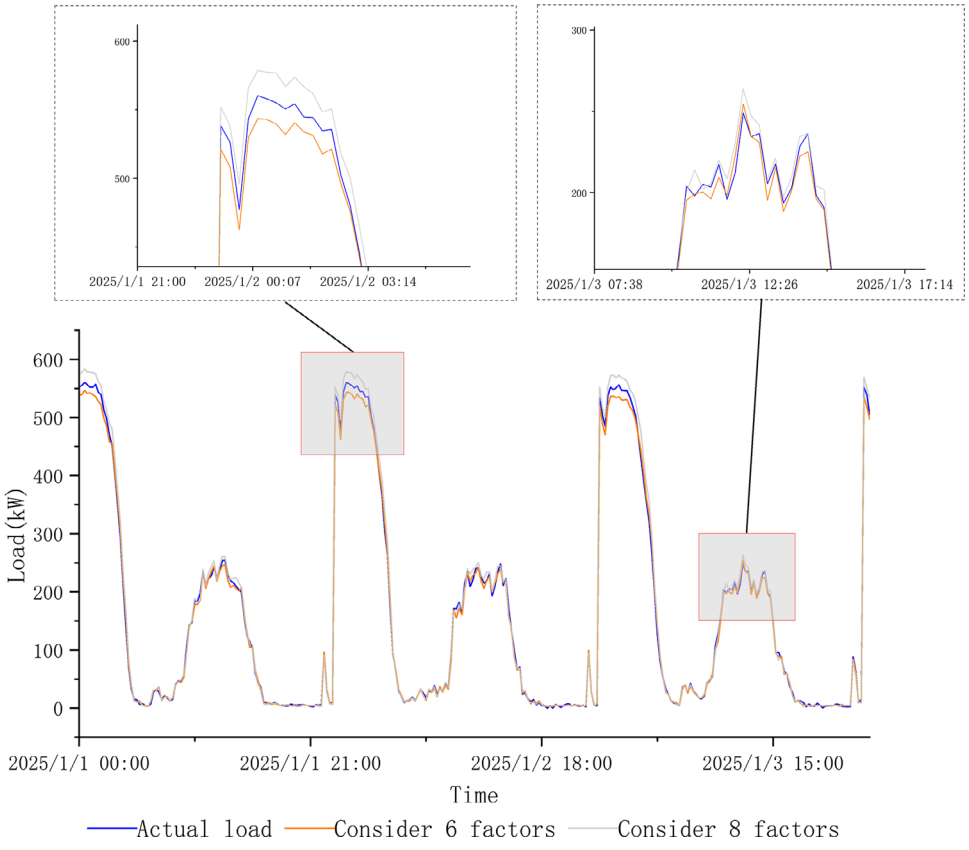


FIGURE 15 | Comparison of model prediction results before and after feature screening.

17518695, 2026, 1, Downloaded from https://ietresearch.onlinelibrary.wiley.com/doi/10.1049/gtd2.70219 by Politecnico Di Torino Sist. Bibl Del Polit Di Torino, Wiley Online Library on [03/11/2026]. See the Terms and Conditions (https://onlinelibrary.wiley.com/terms-and-conditions) on Wiley Online Library for rules of use; OA articles are governed by the applicable Creative Commons License

TABLE 3 | Comparison of model prediction errors before and after feature selection.

Model	Characteristic parameters	MAE (kW)	RMSE (kW)	MAPE (%)
RIME-CNN-LSTM-Attention	After feature screening (6 feature factors)	152.11	12.58	3.22
	No feature screening (8 feature factors)	218.42	19.65	4.62

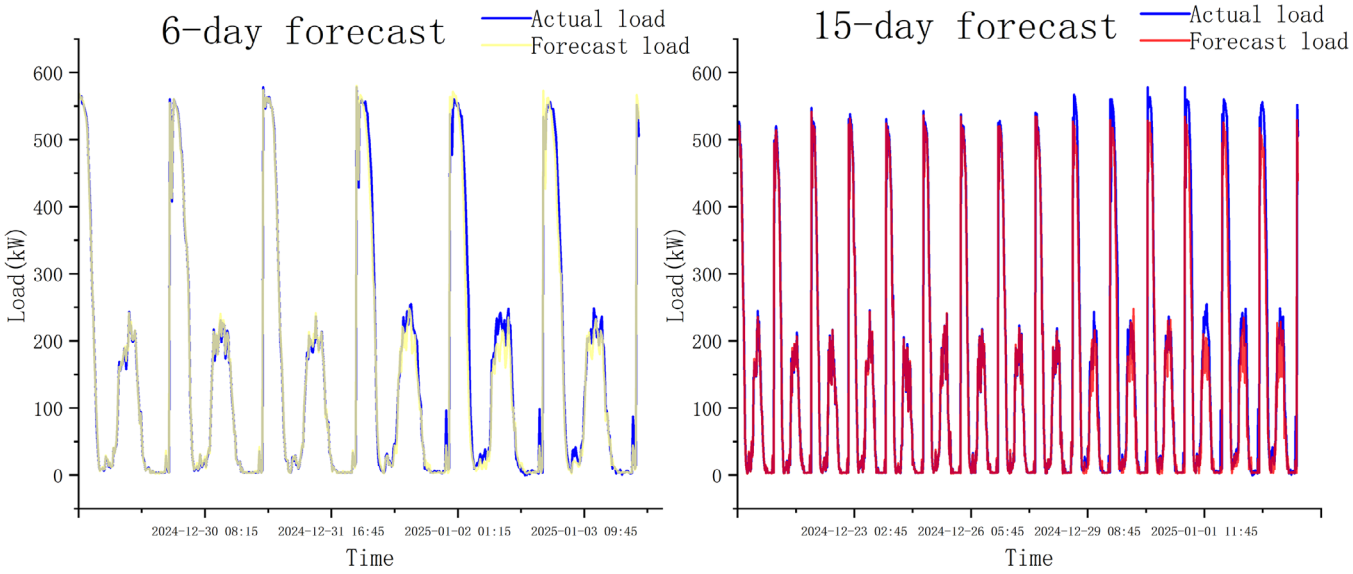


FIGURE 16 | Comparison of model prediction results under different forecasting horizons.

TABLE 4 | Comparison of model prediction errors under different forecasting horizons.

Model	Forecast days	MAE (kW)	RMSE (kW)	MAPE (%)
RIME-CNN-LSTM-Attention	3	152.11	12.58	3.22
	6	718.43	65.15	6.26
	15	953.72	87.34	7.38

In summary, the RIME-CNN-LSTM-Attention hybrid model prediction method based on correlation analysis introduced in this paper achieves greater prediction accuracy compared to alternative models.

6 | Conclusions and Future Work

This paper proposes a RIME-CNN-LSTM-Attention hybrid model prediction method based on correlation analysis. The main conclusions are as follows:

1. Through SPSS25.0 statistical analysis software, based on three correlation analysis methods of Pearson, Spearman and Kendall's tau-b, the variables with weak correlation with the load are screened out, and a highly correlated feature set is constructed. This method simplifies model training complexity and enhances data quality and predictive insight clarity.
2. By integrating CNN, LSTM, and Attention mechanisms, the advantages of CNN in local feature extraction, LSTM in temporal dependency modelling, and Attention in dynamic weighting of key features are fully utilised to construct a deep prediction structure suitable for EV load data, which significantly enhances the model's learning ability for complex nonlinear features.
3. The RIME frost optimisation algorithm is introduced to simulate the soft frost diffusion and hard frost puncture mechanism in nature, realise the global optimal search for CNN and LSTM parameters, overcome the problem of traditional gradient optimisation falling into local optimality, and improve the convergence speed and stability of model training.
4. In comparative studies involving diverse models, the suggested model shows significant advantages in key indicators such as MAE, RMSE, and MAPE; it also shows excellent accuracy and generalisation ability in feature screening

17518695, 2026, 1, Downloaded from https://ietresearch.onlinelibrary.wiley.com/doi/10.1049/gtd2.70219 by Politecnico Di Torino Sist. Bibl Del Polit Di Torino, Wiley Online Library on [03/11/2026]. See the Terms and Conditions (https://onlinelibrary.wiley.com/terms-and-conditions) on Wiley Online Library for rules of use; OA articles are governed by the applicable Creative Commons License

verification and long-term prediction analysis, verifying the stability and practical value of this method.

While the proposed framework demonstrates strong predictive performance, it is important to acknowledge the limitations of the correlation-based feature selection approach. Pearson, Spearman, and Kendall's tau-b coefficients offer an interpretable and computationally efficient way to filter irrelevant inputs, but they primarily capture linear or monotonic relationships between individual features and the target variable. As univariate measures, they may overlook nonlinear interactions and inter-feature dependencies such as multicollinearity. To address these limitations, future work will explore advanced machine learning-based feature selection techniques, including embedded methods (e.g., LASSO, Random Forest), wrapper methods (e.g., Recursive Feature Elimination), and multivariate filters (e.g., mRMR). These approaches can capture complex feature interactions and are expected to yield a more robust and informative input set, further enhancing prediction accuracy and model generalisation.

Author Contributions

Mao Yang: conceptualisation. **Wencheng Li:** writing – original draft. **Peng Sun:** writing – review and editing. **Xin Su:** data curation. **Tao Huang:** methodology. **Tianyu Zheng:** formal analysis.

Acknowledgements

This work was supported by the Xinjiang Uyghur Autonomous Region's Significant Research and Development Program (Grant No. 2022B01020-1).

Conflicts of Interest

The authors declare no conflicts of interest.

Data Availability Statement

Research data are not shared.

References

1. T. Zhang, Y. Huang, H. Liao, and Y. Liang, "A Hybrid Electric Vehicle Load Classification and Forecasting Approach Based on GBDT Algorithm and Temporal Convolutional Network," *Applied Energy* 351 (2023): 121768, https://doi.org/10.1016/j.apenergy.2023.121768.

2. W. Khan, W. Somers, S. Walker, K. de Bont, J. Van der Velden, and W. Zeiler, "Comparison of Electric Vehicle Load Forecasting Across Different Spatial Levels With Incorporated Uncertainty Estimation," *Energy* 283 (2023): 129213, https://doi.org/10.1016/j.energy.2023.129213.

3. Y. Quan and L. Xi, "Smart Generation System: A Decentralized Multi-agent Control Architecture Based on Improved Consensus Algorithm for Generation Command Dispatch of Sustainable Energy Systems," *Applied Energy* 365 (2024): 123209, https://doi.org/10.1016/j.apenergy.2024.123209.

4. M. Yang, Y. Huang, and C. Xu, "Review of Several Key Processes in Wind Power Forecasting: Mathematical Formulations, Scientific Problems, and Logical Relations," *Applied Energy* 377, no. Pt. C (2025): 124361.

5. W. Chen, D. Xu, and R. Guo, "Research on the Influence of Load Forecasting on Multi-objective Optimization Dispatch of New Energy Power Grid," *Power System Protection and Control* 48, no. 10 (2020): 46–51.

6. F. Chen, Y. Wang, H. Deng, Q. Sun, Q. Chen, and Xia, "Probabilistic Prediction of Electric Vehicle Load in Service Area Incorporating Highway Spatiotemporal Traffic Information," *Energy* 329 (2025): 136683, https://doi.org/10.1016/j.energy.2025.136683.

7. Z. Zhou, J. Huang, and R. Zhou, "Charging Pile Load Prediction Using Temporal Convolutional Network With Consideration of Key Meteorological Factors," *Proceedings of the CSU-EPSA* 35, no. 5 (2023): 28–36.

8. M. Arias and S. Bae, "Electric Vehicle Charging Demand Forecasting Model Based on Big Data Technologies," *Applied Energy* 183, no. 2016 (2016): 327–339, https://doi.org/10.1016/j.apenergy.2016.08.080.

9. N. Huang, H. Sun, and S. Wang, "Spatial-temporal Short-Term Prediction of Electric Vehicle Charging Load Considering Differential Coupling Association of Multiple Public Charging Stations," *Proceedings of the CSEE* (2024): 1–12.

10. D. Liu, Y. Zhang, and X. Peng, "Cluster Prediction of Electric Vehicle Charging Load Considering Similar Days and Meteorological Factors," *Electric Power Construction* 42, no. 02 (2021): 43–49.

11. J. Chen, Y. Zou, J. Zhang, and X. Zhang, "Optimal Charging and Discharging Strategy for Workplace Electric Vehicle Charging Stations With Renewable Energy and Power Network Constraints," *Energy* 336 (2025): 138422.

12. W. X. Lin, D. Wu, and B. Boulet, "Spatial-temporal Residential Short-Term Load Forecasting via Graph Neural Networks," *IEEE Transactions on Smart Grid* 12, no. 6 (2021): 5373–5384, https://doi.org/10.1109/TSG.2021.3093515.

13. S. Pang, K. Fan, and C. Chen, "Multi-time Scale Prediction Model of Electric Vehicle Charging Load Based on LightGBM Algorithm and Travel Chain Theory," *Automotive Technology* no. 06 (2024): 9–16.

14. M. Zhang, Q. Sun, and X. Yang, "Electric Vehicle Charging Load Prediction Considering Real-Time Interaction of Multi-source Information and User Regret Psychology," *Power System Technology* 46, no. 02 (2022): 632–645.

15. J. Zheng, M. Dai, and M. Zhang, "Load Aggregation Characteristics and Modeling of Residential Electric Vehicle Charging Stations," *Proceedings of the CSEE* 32, no. 22 (2012): 32–38.

16. S. Bae and A. Kwasinski, "Spatial and Temporal Model of Electric Vehicle Charging Demand," *IEEE Transaction Smart Grid* 3, no. 1 (2012): 394–403, https://doi.org/10.1109/TSG.2011.2159278.

17. Y. Zhang, Z. Zhang, and C. Liu, "Electric Vehicle Charging Load Prediction Based on Dynamic Adaptive Graph Neural Network," *Automation of Electric Power Systems* 48, no. 07 (2024): 86–93.

18. X. Long, J. Yang, and F. Wu, "Electric Vehicle Charging Load Prediction Considering Road Network-grid Interaction and User Psychology," *Automation of Electric Power Systems* 44, no. 14 (2020): 86–93.

19. J. Zhang, J. Yan, and Y. Q. Liu, "Daily Electric Vehicle Charging Load Profiles Considering Demographics of Vehicle Users," *Applied Energy* 274 (2020): 115063, https://doi.org/10.1016/j.apenergy.2020.115063.

20. K. Qian, C. Zhou, and M. Allan, "Modeling of Load Demand due to EV Battery Charging in Distribution Systems," *IEEE Transactions on Power Systems* 26, no. 2 (2011): 802–810, https://doi.org/10.1109/TPWRS.2010.2057456.

21. E. Genov, C. De Cauwer, G. Van Kriekinge, T. Coosemans, and M. Messagie, "Forecasting Flexibility of Charging of Electric Vehicles: Tree and Cluster-based Methods," *Applied Energy* 353 (2024): 121969, https://doi.org/10.1016/j.apenergy.2023.121969.

22. L. G. Maltais and L. Gosselin, "Forecasting of Short-term Lighting and Plug Load Electricity Consumption in Single Residential Units: Development and Assessment of Data-driven Models for Different Horizons," *Applied Energy* 307 (2022): 118229, https://doi.org/10.1016/j.apenergy.2021.118229.

23. Y. Liu, Z. Li, and W. Wei, "Short-Term Charging Load Forecasting of Electric Vehicles Based on LSTM-GNN Combined Model," *Journal of Power Supply* 2024. 1–14.

17518695, 2026, 1, Downloaded from https://ietresearch.onlinelibrary.wiley.com/doi/10.1049/gtd2.70219 by Politecnico Di Torino Sist. Bibl Del Polit Di Torino, Wiley Online Library on [03/11/2026]. See the Terms and Conditions (https://onlinelibrary.wiley.com/terms-and-conditions) on Wiley Online Library for rules of use; OA articles are governed by the applicable Creative Commons License

24. J. Lu, Q. Zhang, and Z. Yang, "Short-term Load Forecasting Method Based on CNN-LSTM Hybrid Neural Network Model," *Automation of Electric Power Systems* 43, no. 08 (2019): 131–137.

25. J. Ren, H. Wei, and Z. Zou, "Ultra-short-term Power Load Forecasting Based on CNN-BiLSTM-Attention," *Power System Protection and Control* 50, no. 08 (2022): 108–116.

26. J. Tian, H. Liu, W. Gan, Y. Zhou, N. Wang, and S. Ma, "Short-Term Electric Vehicle Charging Load Forecasting Based on TCN-LSTM Network With Comprehensive Similar Day Identification," *Applied Energy* 381 (2025): 125174, https://doi.org/10.1016/j.apenergy.2024.125174.

27. O. Tutsoy and C. Tanrikulu, "A Machine Learning-Based 10 Years Ahead Prediction of Departing Foreign Visitors by Reasons: A Case on Türkiye," *Applied Sciences* 12, no. 21: 11163, https://doi.org/10.3390/app122111163.

28. O. Tutsoy, A. Polat, S. Colak, and K. Balikci, "Development of a Multi-Dimensional Parametric Model With Non-Pharmacological Policies for Predicting the COVID-19 Pandemic Casualties," *IEEE Access* 8 (December 2020): 225272–225283, https://doi.org/10.1109/ACCESS.2020.3044929.

29. M. Yang, C. Han, and W. Zhang, "A Short-Term Power Prediction Method for Wind Farm Cluster Based on the Fusion of Multi-source Spatiotemporal Feature Information," *Energy* 294 (2024): 130770, https://doi.org/10.1016/j.energy.2024.130770.

30. M. Yang, X. Shen, and D. Huang, "Fluctuation Classification and Feature Factor Extraction to Forecast Very Short-Term Photovoltaic Output Powers," *CSEE Journal of Power and Energy Systems* 11, no. 02 (2025): 661–670.

31. M. Yang, Y. Guo, and B. Wang, "A Day-ahead Wind Speed Correction Method: Enhancing Wind Speed Forecasting Accuracy Using a Strategy Combining Dynamic Feature Weighting With Multi-source Information and Dynamic Matching With Improved Similarity Function," *Expert Systems With Applications* 263 (2025): 125724, https://doi.org/10.1016/j.eswa.2024.125724.

32. B. Tan, Z. Liang, C. Y. Chung, H. Tan, H. Wang, and H. Yang, "Risk-based Data-driven Energy Management for Integrated Electrical and Hydrogen Microgrids With Improved Hydrogen Vehicle Charging Prediction," *Applied Energy* 398 (2025): 126410, https://doi.org/10.1016/j.apenergy.2025.126410.

33. H. Su, D. Zhao, and H. Aliasghar, et al., "RIME: A Physics Based Optimization," *Neurocomputing* 532 (2023): 183–214, https://doi.org/10.1016/j.neucom.2023.02.010.

34. Y. He, H. Jin, and C. Zhou, "Research on Non-invasive Blood Glucose Prediction Model Based on RIME and 1DCNN-LSTM-Attention," *Modern Electronic Technology* 47, no. 18 (2024): 83–88.

35. Y. Liu and Q. Zhao, "CNN-LSTM Ultra-short-term Power Load Forecasting Based on Clustering Empirical Mode Decomposition," *Power System Technology* 45, no. 11 (2021): 4444–4451, https://doi.org/10.13335/j.1000-3673.pst.2021.0016.

36. K. Ping-Huan and H. Chiou-Jye, "A High Precision Artificial Neural Networks Model for Short-Term Energy Load Forecasting," *Energies* 11, no. 1 (2018): 213–226.

37. B. Zhao, Z. Wang, and W. Ji, "CNN-GRU Short-Term Power Load Forecasting Method Based on Attention Mechanism," *Power System Technology* 43, no. 12 (2019): 4370–4376, https://doi.org/10.13335/j.1000-3673.pst.2019.1524.

38. P. Li, S. He, and P. Han, "Short-Term Load Forecasting of Smart Grid Under Real-Time Electricity Price Conditions Based on Long Short-Term Memory," *Power System Technology* 42, no. 12 (2018): 4045–4052.

39. S. Jung, J. Moon, and S. Park, "An Attention-based Multilayer GRU Model for Multistep-ahead Short-Term Load Forecasting," *Sensors* 21, no. 5 (2021): 1–20, https://doi.org/10.3390/s21051639.

40. M. Yang, Y. Guo, and F. Fan, "Ultra-short-term Prediction of Wind Farm Cluster Power Based on Embedded Graph Structure Learning With Spatiotemporal Information Gain," *IEEE Transactions on Sustainable Energy* 16, no. 01 (2025): 308–322, https://doi.org/10.1109/TSTE.2024.3455759.

41. M. Yang, Y. Jiang, and C. Xu, "Day-ahead Wind Farm Cluster Power Prediction Based on Trend Categorization and Spatial Information Integration Model," *Applied Energy* 388 (2025): 125580, https://doi.org/10.1016/j.apenergy.2025.125580.

42. Z. Liu, L. Xi, Y. Quan, and C. Cheng, "Brain-inspired Collaborative Power Dynamic Dispatch for the Digital Twin Smart Generation System," *IEEE Transactions on Industry Applications* 61, no. 1 (2025): 1420–1430, https://doi.org/10.1109/TIA.2024.3373371.

43. M. Yang, Y. Huang, Z. Wang, B. Wang, and X. Su, "A Framework of Day-Ahead Wind Supply Power Forecasting by Risk Scenario Perception," *IEEE Trans Sustain Energy* 16, no. 3 (2025): 1659–1672, https://doi.org/10.1109/tste.2025.3525498.

44. M. Yang, R. Jiang, B. Wang, G. Fang, Y. Jia, and F. Fan, "Multi-channel Attention Mechanism Graph Convolutional Network Considering Cumulative Effect and Temporal Causality for Day-ahead Wind Power Prediction," *Energy* 332 (2025): 137023, https://doi.org/10.1016/j.energy.2025.137023.

45. J. X. Che and J. Z. Wang, "Short-Term Load Forecasting Using a Kernel-based Support Vector Regression Combination Model," *Applied Energy* 132 (2014): 602–609, https://doi.org/10.1016/j.apenergy.2014.07.064.

46. S. Han, F. Hu, and Z. Chen, "Day-ahead Market Marginal Electricity Price Prediction Based on GCN-LSTM," *Proceedings of the CSEE* 42, no. 9 (2022): 3276–3286.

17518695, 2026, 1, Downloaded from https://ietresearch.onlinelibrary.wiley.com/doi/10.1049/gtd2.70219 by Politecnico Di Torino Sist. Bibl Del Polit Di Torino, Wiley Online Library on [03/11/2026]. See the Terms and Conditions (https://onlinelibrary.wiley.com/terms-and-conditions) on Wiley Online Library for rules of use; OA articles are governed by the applicable Creative Commons License